Title
Stochastic excitation of seismic waves by a hurricane

Author
Tanimoto, Toshiro

Publication Date
2015-10-01

Stochastic excitation of seismic waves by a hurricane

Toshiro Tanimoto* and Anne Valovcin

Department of Earth Science and Earth Research Institute,

University of California, Santa Barbara, California 93106, USA.

*Corresponding author: Email toshiro@geol.ucsb.edu

Abstract

We investigate how a tropical cyclone (Hurricane Isaac in 2012) generated seismic ground motions using seismic and barometric data from the Earthscope network. In the frequency band 0.01-0.02 Hz, seismic and surface-pressure amplitudes show a systematic decreasing trend with distance from the center of the hurricane. However, the decreasing rate is much higher for seismic waves than for pressure. We develop a stochastic theory of seismic-wave excitation by surface pressure that connects these two observed data sets; surface pressure is the excitation source and seismic data are the resulting seismic-wave field. This theory contains two parameters: (i) the pressure power spectral density (pressure PSD, S_p) and (ii) the correlation length in the pressure field (L). Using the formula, we solve for the spatial variation of correlation lengths. The solution shows that longer correlation lengths in pressure are near the hurricane center. Because seismic-wave excitation is proportional to $L^2 S_p$, the excitation for seismic waves becomes effectively more localized closer to the center. Also the scaling relation between L and S_p leads to an excitation source which is approximately proportional to the third power of surface pressure. This centralized source for seismic-wave excitation explains why the

decreasing rate with distance is higher for seismic data than for barometric data. However, this spatial-coherence mechanism may not be the only process, as strong turbulence near the center may cause transient bursts of pressure and also induce higher temporal correlation. These alternative mechanisms need to be carefully analyzed in the future.

1. Introduction

The idea of monitoring hurricanes (tropical cyclones) by seismic data has a long history [e.g., Gilmore and Hubert, 1946]. The main purpose then was to detect hurricanes from the use of microseisms [Oroville and Gutenberg, 1946] but such a seismic approach was soon replaced by satellite observations from space. With the appearance of broadband seismometers and their arrays in the last 20 years, the number of seismic studies on hurricanes has increased again. This was motivated by an interest that global warming and increased hurricane power may be related, and seismic data may have an answer [e.g., Bromirski and Kossin, 2008; Ebeling and Stein, 2011].

The aim of this study is to understand how an on-land hurricane excites seismic ground motions. Many recent seismic studies on hurricanes examined data while hurricanes were still in the ocean [e.g., Zhang et al., 2010; Chi et al., 2010; Lee et al., 2012] which makes our study quite different from them. We take full advantage of the Earthscope network (www.earthscope.org), which consists of permanent stations, and the Transportable Array (TA hereafter), which has a dense distribution of barometers and seismometers. This network has recorded unique data for hurricanes in the last 5-6 years as some hurricanes passed directly through this network. This is an ideal situation to study on-land hurricanes as barometer data provide information on the excitation source of seismic waves and seismic data provide the resultant seismic wave fields.

In this study, we focus on Hurricane Isaac in 2012. We conducted a preliminary study on it [Tanimoto and Lamontagne, 2014, hereafter TL14] using seismic data only. By inverting seismic data for surface pressure, TL14 led to a solution that indicated large pressure changes under the eyewall of the hurricane. Time evolution (decay) of this surface pressure solution suggested a particular manner by which this eyewall system decayed. We discussed that this time evolution must be related to the changes in the ascending flow in the eyewall which deteriorated over a few days after landfall [Riehl, 1950; Jorgensen, 1984; Jorgensen et al., 1985; Emanuel, 1986, 1991, 1997, 2003].

In order to connect and understand seismic and barometric data, we develop a stochastic excitation theory which extends the normal-mode excitation theory [e.g., Gilbert, 1970; Dahlen and Tromp, 1998]. Stochastic excitation theories based on the normal-mode approach were developed previously for various problems, such as for the Sun's oscillations [Goldreich and Keeley, 1977] and for long-period seismic noise, often referred to as the hum [Kobayashi and Nishida, 1998; Fukao et al., 2002; Tanimoto, 1999, 2005, 2013; Tanimoto and Um, 1999; Webb, 2007, 2008; Gualtieri et al., 2013]. The approach in this paper is closest to Fukao et al. [2002]. However, Fukao et al. [2002] worked on a global-scale problem while a hurricane problem is a regional one (horizontal scale ~1000km), which requires a different approximation at the last step.

Our main approach is to examine the amplitude-distance variations of seismic and pressure data from the hurricane center and monitor their time evolution where we discovered the amplitude decay rate with distance is faster for seismic data than for pressure data. This study centers on this observation and attempts to answer this difference through data analysis. In particular, we propose a mechanism in which the correlation length in the pressure field becomes larger near the center of a hurricane; in general, a longer correlation length in the (random) pressure field increases the efficiency of seismic-wave excitation. Longer correlation length near the center essentially leads to a more centrally focused source than the original pressure field and can explain the differences in decay rates with distance.

In essence, we invoke higher spatial coherence in the surface-pressure field near the hurricane center to explain the observation. A centrally focused source may arise by different mechanisms, however; for example, due to strong turbulence near the center, transient bursts of pressure may occur. A higher temporal coherence may also result. Both mechanisms may lead to a similar centralized source. We briefly discuss such alternative mechanisms in the discussion, although detailed analyses of these mechanisms are beyond the scope of this paper.

We will describe the basic information on Hurricane Isaac in section 2, some key features in seismic and barometric data in section 3, and present our stochastic excitation theory in section 4. In section 5, we show our attempts to fit seismic and barometric data **to** this theory and how the correlation length in this stochastic excitation theory is estimated from data. In section 6, we present a scaling analysis from the derived solutions in section 5 and show the excitation source effectively becomes proportional to the third power of pressure near the center. We will briefly discuss the alternative mechanisms in section 7 and summarize our conclusions in section 8.

2. Hurricane Isaac

Figure 1 shows the track of Hurricane Isaac based on satellite data [Berg, 2013]. This information is critical for our analysis as we use these locations for constructing the amplitude-distance plots for each time interval.

Hurricane Isaac in 2012 was a tropical storm for most of its life but it intensified to become a hurricane at about 12:00 UTC August 28, twelve hours before its first landfall at the mouth of the Mississippi river, and remained a hurricane until about 18:00 August 29. Its hurricane stage (category 1) is indicated by red circles in Figure 1. Its first landfall occurred at 00:00 UTC August 29. The eye crossed back over the nearby ocean but stayed very close to the coast. The second landfall occurred at 08:00 UTC August 29, just west of Port Fourchon, Louisiana. After the second landfall, it moved northward in an area dense with seismometers and barometers from the Earthscope project. Hereafter, when we refer to the landfall, we refer to the second landfall at 08:00 UTC on August 29.

3. Amplitude-Distance Plots from Hurricane center

(3.1) Examples of seismic and barometric data

We pointed out in TL14 that one of the difficulties in studying the strength of a hurricane by seismic waves is that not all seismic waves come directly from the center of a hurricane. For some frequency bands, ocean waves which are excited by the same hurricane become secondary sources of seismic-wave excitation [Longuet-Higgins, 1950; Hasselmann, 1963]. Evidence was shown in TL14 that this was indeed the case for seismic waves for frequencies about 0.1-0.3 Hz. This is unfortunate because this band is the most energetic frequency band of seismic waves, but in order to study the processes near the hurricane center, we must focus on other frequency bands.

In TL14, we also showed that processes near the hurricane eye are the dominant source of low-frequency seismic waves **of** about 0.01-0.02 Hz. Figure 2 shows seismic and barometric data for Hurricane Isaac at 00:00 UTC on August 30. We computed the power spectral density (PSD) by using the formula $|F(\omega)|^2/T$ where $F(\omega)$ is the Fourier spectra of seismograms (ground velocity) and T is the length of time series. For this study, we used $T=1$ hour for all computation of PSDs.

In this paper, we only analyze vertical-component seismograms (as in TL14) and barograms. Horizontal-component seismograms have large amplitudes but also contain large scatter and we feel we are not at a stage to understand the behaviors of horizontal-component data. Vertical components show much more systematic amplitude variations with smaller scatter and we believe that an understanding between barometer data and vertical component seismograms is possible.

The left panels in Figure 2 show seismic amplitudes (PSD) on a map (top) and the amplitude-distance plot from the hurricane center (bottom). The hurricane center is shown by the red triangle in the top panel. The two right panels show similar plots for surface pressure. The concentric circles from the center are drawn at every 100 km (top) and the same color scales are used for the top and the bottom panels.

In both seismic and pressure data, we note that high-amplitude stations (red) tend to surround the hurricane center (top panels). This indicates that the exciting sources of these waves are near the center of this hurricane. They approximately show axisymmetric patterns, although some deviations may be recognized. Because of these observed features, we adopt an axisymmetric assumption in the theory and also in the data analysis.

In the two bottom panels, both spanning 0-1000 km from the center, show an important difference between seismic and pressure data. That is, the differences in the rates of amplitude decay with distance from the center. Seismic data merge with the background noise at about 500-600 km beyond which amplitudes flatten out (Figure 2, bottom-left). A black dashed line is shown in the figure in order to indicate the background noise level. Pressure data merge with the background noise at about 800-1000 km (Figure 2, bottom-right). The amplitude-distance decay rate is clearly higher for seismic data than that for barometric data. This is one of the most important features that we seek to explain by our analysis.

(3.2) Amplitude-distance plots

In Figure 3 (a-h), we show how seismic amplitudes (PSD) in the frequency band 0.01-0.02 Hz varied with distance from the center of Hurricane Isaac. These plots are the snapshots of the amplitude-distance plots after the landfall. With respect to the second landfall (UTC 08:00 Aug. 29), they start from -2 hours (2 hours before landfall) to 40 hours after landfall plotted at 6 hour intervals from Figure 3a to Figure 3h.

In the first two panels (Figures 3a and 3b), the seismic amplitude peak is sharp and is located at a distance about 70-80 km from the center. A vertical dash line is given in each panel to indicate the distance of 75 km. At the 10th hour (Figure 3c), the peak value had decreased by a factor of two and the width of the peak became slightly broader but the peak location stayed at about the same distance from the hurricane center. At the 16th hour (Figure 3d) the peak still stayed close to 70-80 km but the width of the peak had clearly increased. At the 22nd hour (Figure 3e) and the 28th hour (Figure 3f) the widths of the peak became much wider with increased scatter in seismic amplitudes and at the same time the peak distance from the center increased. At the 34th hour (Figure 3g), a broad peak at a distance of about 300 km can be recognized but the scatter is now quite large. Scatter in amplitudes become even larger at the 40th hour (Figure 3h).

Figures 4a-4h show the surface pressure PSD vs. distance from the hurricane center. Each panel is at the same time interval with Figures 3a-3h. In general, pressure data contain larger scatter than seismic data. They also show a smaller decay rate with distance, as we noted in Figure 2. Note that these hurricane-related signals merge with the background pressure (PSD) noise level at about 800-900 km from the center and this merging occurs at about the same distance for all time intervals in Figures 4a-4h.

We note that the background noise level became higher in Figure 4c and Figure 4g in comparison to other cases, but even in these data a merging distance with the background seems to occur at about the same distance. An increased level of seismic background noise is seen in Fig. 3f and also in Fig. 3g but we believe that they were caused by M~7 earthquake that occurred elsewhere at about this time (near the Jan Mayen Is.). Large teleseismic earthquakes can raise the background seismic noise level for the frequency range 0.01-0.02 Hz because of long-period surface waves that circle around the Earth. However, there is no reason for barometer data to be affected by teleseismic events. We speculate that there were atmospheric conditions that led to higher pressure PSDs for these time intervals but strictly speaking, we do not know why they occurred in Figures 4c and 4g. However, in our analysis, we will focus on the distance range 0-400 km where signals in both data sets are clearly controlled by the hurricane. We believe these differences in background noise levels will not affect our conclusions.

(3.3) Seismic PSD vs. Pressure PSD at same stations

In Figure 5, we show a plot of seismic PSD vs. pressure PSD from the same stations. Stations within 500 km of the hurricane center are plotted at three different time intervals (6:00, 12:00, 18:00 on August 29). For reference, two lines with the power of 1.5 (dash) and 2 (blue) are shown.

Figure 5 emphasizes that the relationship between seismic PSD and pressure PSD are not linear. For propagating waves from the 2003 Tokachi-Oki earthquake, Watada et al. (2006) showed that seismic amplitude and pressure amplitude were related by a transfer function, which is an example of a linear relation. This was because both pressure and seismic waves were properties of propagating waves. For our hurricane problem, the relationship is clearly more complex as pressure is the excitation source and seismic waves are the resulting field.

(3.4) Averaging for seismic PSD and pressure PSD

For later analysis, instead of working with the raw data in Figures 3a-3h and 4a-4h, we took the average PSDs for both data sets. The averaging was done in the following way; first we take a 50-km interval and identify the raw data within this interval. Let us denote raw data within this distance range by x_i (distance) and y_i (PSD) with i=1,2,…,n. We took the average of them and treating it as the data point for this 50-km range. We shifted the 50-km window by every 10 km and applied the same procedure. Near the center (smaller distance range), data are relatively sparse and this procedure sometimes yielded the same values for adjacent spatial windows. We removed such redundancy in the averaged data and linearly interpolated the averaged data for every 5 km.

This averaging was done in linear numbers rather than in logarithms. Our later analyses are done for these linearly averaged numbers. Therefore, some of the features in small numbers seen in the logarithm plots, that show 3-4 orders of magnitude variations (Figures 3 and 4), may not be represented well in these averages. We believe that the most important features of a hurricane are in large-amplitude signals and we attempt to understand them, typically closer to the center of a hurricane.

Figure 6 shows an example of the averaging process at 00:00 UTC on August 30. The original data, from Figures 3d (seismic data, top) and 4d (pressure data, bottom) are shown in black. The averaged data is shown in blue and the interpolated data is shown in red. When a blue circle and a black circle overlaps, it is shown by blue in these figures. The averaged PSDs seem to capture most of the long wavelength features in the original data which we seek to understand in this paper.

We added the points at distance 0 km with zero amplitudes in these analyses. This addition is justified for the pressure data as pressure is very low at the center of a hurricane. For seismic data, amplitudes may not necessarily go to zero, although it should also be smaller than those outside the eyewall because the center of a hurricane is a calm region. In the following analysis, we only use data for distances larger than 50 km (up to 400 km) and these added points at distance zero do not affect our results very much.

Figure 7 shows the summary of averaged PSDs where the top panel shows seismic PSDs for eight time intervals and the bottom panel shows pressure PSDs for the same time intervals. Here, as observed in Figures 3 and 4, higher decay rates with distance for seismic data than those for pressure data can be confirmed in those averaged PSDs.

(3.5) Coherence in the atmospheric pressure field

For the excitation of seismic waves by atmospheric pressure, the source is almost like a random force, distributed over an area, and the correlation length in the pressure field becomes a key parameter for the efficiency of excitation. The correlation length is generally considered to be short and is less than 1 km (Herron et al., 1969; McDonald et al., 1971; Nishida et al., 2005), but it may vary with frequency. Since the short coherence length is the critical assumption in the derivation of theoretical formulae, we examined it for our barometric data.

Figure 8 shows the coherence for pairs of barometric stations in the TA, plotted against distance between stations. The top figure was computed for a two-hour time interval centered at 12:00 on August 29, only four hours after the landfall and while the hurricane was still quite strong. The coherence between two stations, whose spectra are $X(\omega)$ and $Y(\omega)$, was computed by $E[X^*(\omega)Y(\omega)]/\sqrt{E[X^*(\omega)X(\omega)]E[Y^*(\omega)Y(\omega)]}$, where the stars denote complex conjugation. The ensemble averages E[ ] were taken by using different overlapping time windows with 30-minute length. Figure 8 shows the case when 18 time windows, each shifted by five minutes, were used (over a span of two hours). We then averaged these coherence values between 0.01 and 0.02 Hz. Results at 18:00 on August 29 are also shown in the bottom panel.

The results in Fig. 8 indicate that there is no meaningful coherence among barometric data; this is not surprising since a typical distance between adjacent stations in the Transportable Array is 70 km. This does not prove that the correlation length is about 1 km or less but it confirms that the data are consistent with short correlation lengths in the atmospheric pressure field.

4. Theory of Stochastic Excitation of Seismic Ground Motion

In this section, we derive a formula that relates the seismic PSD to the pressure PSD. First we state the final formula; it can be written in the form

$$S_{\mathrm{v}}(x,\omega) = \int K(x,x_s,\omega) S_p(x_s,\omega) dx_s \tag{1}$$

where $S_{\mathrm{v}}(x,\omega)$ is the PSD of observed seismic ground velocity at distance x from the center of a hurricane (angular frequency ω), $S_p(x_s,\omega)$ is the surface pressure PSD at x_s, and $K(x,x_s,\omega)$ is the kernel that we can compute for a given Earth model. The integration variable x_s is the source distance measured from the center of a hurricane. The integration arises because the pressure source is distributed over a large area.

The main steps for the derivation of equation (1) proceed as follows. Let us denote the excitation source (that is surface pressure) by $\delta p(\theta_S,\phi_S,t')$. This pressure is distributed over a broad area on the surface of the Earth. The source has also acted continuously over time. When multiplied by the surface area, this pressure becomes a surface vertical force. Vertical seismic ground velocity by such a vertical force can be written by

$$\mathrm{v}_z(\theta,\phi,t) = \int d\theta_S \int d\phi_S \sin\theta_S R^2 \sum_{n,l,m} U_n^2(R) Y_l^m(\theta,\phi) Y_l^{m*}(\theta_S,\phi_S)$$

$$\text{x} \int_{-\infty}^{t} dt' e^{-\omega_i (t-t')/2Q_i} \cos\omega_i (t-t') \delta p(\theta_S, \phi_S, t') \qquad (2)$$

where we use the normal mode theory for a layered spherical earth (Gilbert, 1970; Dahlen and Tromp, 1998). The integrations over the colatitude θ_S and the longitude ϕ_S are carried out for the Earth's surface (that is the extent of the pressure source). The integration with respect to time (t') indicates that this pressure source has acted from $t' = -\infty$ to t. R is the radius of the Earth, $Y_l^m(\theta,\phi)$ is the spherical harmonics (e.g., Edmunds, 1960), $U_n(R)$ is the surface value of the vertical eigenfunction for a spheroidal mode with a mode number i=(n,l,m) which is normalized by $I = \int_0^R \rho\{U^2 + l(l+1)V^2\} r^2 dr$. The overtone number is n, the angular degree and order of a spherical harmonics are l and m, and ω_i and Q_i are the eigenfrequency and the attenuation parameter of this mode. The formula contains $U_n^2(R)$ because both the excitation source and a seismograph are at the Earth's surface.

From (2), we form the auto-correlation function of ground velocity

$$C_{\text{v}}(\theta,\phi,\tau) = \frac{1}{T} \int_{-T/2}^{T/2} \text{v}_z(\theta,\phi,t) \text{v}_z(\theta,\phi,t+\tau) dt \,. \qquad (3)$$

Using the relation that Fourier transformation of an auto-correlation is its power spectral density (PSD), we have

$$S_{\text{v}}(\theta,\phi,\omega) = \int_{-\infty}^{\infty} C_{\text{v}}(\theta,\phi,\tau) e^{-i\omega\tau} d\tau \;, \qquad (4)$$

Substituting (2) in (3) and then (3) in (4), the cross-correlation function of surface pressure between $(\theta_{s'},\phi_{s'})$ and $(\theta_{s''},\phi_{s''})$ emerges:

$$C_p(\theta_{s'},\phi_{s'},\theta_{s''},\phi_{s''},\tau)=\frac{1}{T}\int_{-T/2}^{T/2}\delta p(\theta_{s'},\phi_{s'},t)\delta p(\theta_{s''},\phi_{s''},t+\tau)dt \tag{5}$$

By defining the cross power spectral density of pressure by its Fourier transformation

$$S_p(\theta_{s'},\phi_{s'},\theta_{s''},\phi_{s''},\omega)=\int_{-\infty}^{\infty}C_p(\theta_{s'},\phi_{s'},\theta_{s''},\phi_{s''},\tau)e^{-i\omega\tau}d\tau\ , \tag{6}$$

we obtain the following expression,

$$S_{\mathrm{v}}(\theta,\phi,\omega)=\int d\theta_{s'}\int d\phi_{s'}\int d\theta_{s''}\int d\phi_{s''}\sin\theta_{s'}\sin\theta_{s''}R^4$$

$$\sum_{l'}\sum_{l''}\frac{2l'+1}{4\pi}\frac{2l''+1}{4\pi}U_{l'}^2U_{l''}^2\gamma_{l'}\gamma_{l''}^{*}P_{l'}(\cos\Delta')P_{l''}(\cos\Delta'')S_p(\theta_{s'},\phi_{s'},\theta_{s''},\phi_{s''},\omega) \tag{7}$$

where

$$\gamma_{l'}=\frac{(\omega_{l'}/2Q_{l'}-i\omega)}{\{(\omega_{l'}/2Q_{l'}-i\omega)^2+\omega_{l'}^2\}} \tag{8}$$

for l'. Substitution of l'' in l' gives the expression for $\gamma_{l'}$. Δ' is the distance between the observation point (θ,ϕ) and a source $(\theta_{s'},\phi_{s'})$ and Δ'' is the distance between the observation point (θ,ϕ) and a source $(\theta_{s''},\phi_{s''})$. Here we restricted to the fundamental modes only as the overtones are not excited very well by surface forces.

Under the assumption that the correlation length in the surface pressure field is much smaller than the wavelength of seismic waves, we can simplify equation (7) further. This condition is satisfied in our problem because the wavelengths of seismic waves are over 100 km for the frequency range 0.01-0.02 Hz whereas the correlation lengths of pressure are of the order of 1 km or smaller for this frequency range [e.g., Herron et al., 1969; McDonald et al, 1971, Nishida et al., 2006]. Figure 8 lends some support for this assumption. We can then approximate the double surface integrals in (7) by a single surface integral multiplied by πL^2 where L is the correlation length. This approximation means that if two points are within the distance L, the correlation in the pressure field is 1 but otherwise it is 0.

We also introduce the assumption of axisymmetry into this problem as we discussed with Figure 2. Equation (7) can then be approximated by

$$S_v(x,\omega) = \int K(x,x_s,\omega) S_p(x_s,\omega) dx_s \tag{9}$$

where the kernel is explicitly written by

$$K(x,x_s,\omega) = \frac{L^2}{4\pi} R \sin\theta_s' \sum_{l'} \sum_{l''} (l'+1/2)(l+1/2) U_{l'}^2 U_{l''}^2 \gamma_{l'} \gamma_{l''} \int P_{l'}(\cos\Delta') P_{l''}(\cos\Delta') d\phi_s \ . \tag{10}$$

In this formula, x_s is the distance from the center of a hurricane and the integration with respect azimuth is now in the kernel. Under this assumption, the pressure PSD S_p has an axisymmetric form whose example is shown in Figure 9a. In (10), $x = R\theta$ is the distance from the hurricane center to a seismograph on the surface of the Earth, $x_s \equiv R\theta_s'$ is the distance from the hurricane center to a pressure source (which is distributed over the surface) and Δ' is the distance between the observation point (θ,ϕ) and a source (θ_s,ϕ_s). Using the eigenfunctions and eigenfrequencies of PREM (Dziewonski and Anderson, 1981), we numerically evaluate equation (10). Examples of kernels for sources at $x_s = 50 - 350$ km are shown for every 50 km in Figure 9b. Note that the sources are on a concentric circle at each distance as the integrations with respect to azimuth were already performed. We used L=1 km for these computations.

5. Solving for the correlation length

From the Earthscope network, we have S_v and S_p in (1). In our analysis, we use the averaged PSDs in Figure 7 for these observed quantities. We quickly found out that the relation in (9) cannot fit the data well if the correlation length were constant. Therefore we sought spatially varying correlation length L^2 that can satisfy the two data.

In order to obtain L^2, we formulated an inverse problem whose unknown parameter is this correlation length. This parameter is buried in the kernel in equation (10). We now rewrite the equation as

$$S_v(x) = \int \overline{K}(x, x_s) S_p(x_s) L^2(x_s) dx_s \qquad (11)$$

where $\overline{K}$ is the same with (10) except that L^2 is taken out of the formula and is explicitly shown in the integrand. We used this equation to solve for the correlation length where $L^2(x_s)$ is a function of the distance from the center of the hurricane. Since the quantities S_v and S_p were averaged between 0.01 and 0.02 Hz, we used the averaged kernel for the same frequency band and thus the resultant correlation length should also be interpreted as an averaged quantity.

In order to solve this problem, we discretized the integral in (11) at every 5 km from the distance 50 km to 400 km. The results of inversion for the first four time intervals are shown in Figures 10a-10d. They are at UTC 06:00 (10a), 12:00 (10b), 18:00

(10c) on August 29 and UTC 00:00 (10d) on August 30. Each solution consists of three panels; the obtained correlation lengths with error bars are shown in the top panel, comparison of the observed (averaged) seismic PSDs (red) and the theoretical PSDs (dashed blue) are in the middle panel and the pressure PSDs are in the bottom panel. The solution was obtained by minimizing the differences between the two curves in the middle panel. The red lines in the middle panels and the pressure PSDs in the third panels are the same with those shown in Figure 6. Note that these plots are all in linear, not in log.

In Figures 10a-10d, the correlation lengths have large values for distances less than 200 km and become small beyond 200 km. The maximum correlation length is 1.5 km when the hurricane was mature and strong (Figure 10a) but became small over time as Hurricane Isaac lost its energy after the landfall. The fact that the correlation length becomes large near the center of the hurricane is the most characteristic features in these solutions.

This inversion problem required regularization. We used a simple diagonal damping parameter with first-derivative smoothing for adjacent (5-km) blocks. Examples of the trade-offs between the solution norms and the variance (misfits) are shown in Figure 11. They are for the first two time intervals (Figures 10a and 10b) and the chosen damping parameters are indicated by the red circles. A different choice of damping parameter changes solutions to some extent but as long as a damping parameter is selected near the red circle, solutions are fairly stable.

We did not use the positivity constraint for solving this problem. If a selected damping parameter is too small, a solution often contained some negative regions.

Selected damping parameters give basically zero solutions beyond certain distances (typically 250 km). Replacing those large-distance solutions by zeros does not significantly change the fit.

6. The cubic model

We searched for characteristic features in the solutions; one of the most interesting features is the existence of a correlation between L^2 and the pressure PSD S_p. In Figure 12, we show three different cases of inversion results with different damping parameters. The bottom figure shows our chosen solution, but two other cases are shown to emphasize the robustness of our solutions. The damping parameter is 100 times smaller for the top panel and is 10 times smaller for the middle panel.

The data points in Figure 12 suggest existence of a systematic trend between L^2 and the pressure PSD S_p. We also show the least squares formula (log-log linear) that fit the data. In the formulas shown in these figures, x is $\ln(L^2)$ and y is $\ln(S_p)$. The numbers in the parentheses are the standard deviations (one sigma). We find that the coefficient of x stays close to 0.5 for all three cases (0.516, 0.497, 0.536) despite the fact the damping parameter varied by a factor of 100.

What does a gradient of 0.5 mean in this least-squares solutions? Since x is $\ln(L^2)$ and y is $\ln(S_p)$, it obviously means that $L \propto S_p$. Let us introduce the proportionality constant α and write this relation by $L = \alpha S_p$. This relation means that, since the excitation is proportional to $L^2 S_p$, the excitation source essentially becomes proportional to S_p^3. If we rewrite equation (11) by using this relation, we get

$$S_v(x) = \alpha^2 \int \overline{K}(x, x_s) S_p^3(x_s) dx_s \quad (12)$$

The integrand shows that the excitation of seismic waves becomes proportional to the third power of the pressure. We refer to this as the cubic model.

We refitted the data (the bottom case in Figure 12) by the least-squares method by fixing the gradient at 0.5 and varying only the proportionality constant. The formula we obtained is

$$\ln(S_p) = 0.5\ln(L^2) + 6.572$$

and is also shown in the bottom panel of Figure 13. This formula essentially means that we have a relation

$$L = (1/714.8) S_p(x)$$

where the unit for L is m and the unit for S_p is m^2/s. The constant 714.8 is equal to $e^{6.572}$. Using this relation, we computed theoretical values for this cubic model using (12). Comparison between theory and data is shown in Figure 13 (top). If our theory and observations match, the points should lie on the dashed line in this figure. There are certainly some scatters in this plot but this cubic model seems to explain a major trend in data.

A caveat for this cubic model is that it is a better model for large pressure region or equivalently for small-distance range. Typically the fits are good for distances less than 250 km. The bottom panel of Figure 13 shows that the scatter of points from the least-squares line becomes large for small correlation lengths. But since the dominant signals are from the distance range 0-250 km, the cubic model seems to capture important characteristics of the excitation process.

7. Discussion

(7.1) Alternative mechanisms

In this study, we identified one key observational feature, the difference in decreasing rates with distance between seismic and barometric data. We attributed these differences to variations in the correlation length in the pressure field as a function of distance from the center of the hurricane. However, there can be other possibilities that may explain the observational feature**.** We will discuss two possible mechanisms below.

One mechanism is the transient sources (pressure changes) close to the hurricane center. As strong winds blow into the small, central area of a hurricane, it seems natural to expect transient (intermittent) pressure changes because of strong turbulence. If they occurred frequently, we could have an effectively centralized source for seismic-wave excitation. In order to examine this point, we created amplitude (PSD)-distance plot for every hour (Figure S1) from 00:00, August 29 to the end of August 31. Hourly changes in these plots indicate that there exist some variations, suggesting some stochastic effects in pressure values. But we do not necessarily see a larger number of sudden changes closer to the center; stochasticity seems to be found regardless of distance from the center. But these data are limited, especially because we can only get a limited number of stations close to the center. Clearly a more careful analysis is required.

The second mechanism is the high temporal coherence close to the center. Instead of spatial coherence, temporal coherence may also increase when strong winds blow into a small, central area of a hurricane. If this happens, there will be a centralized source that can explain the observed feature. Although this mechanism is possible, the small number of barometric stations close to the center makes it hard to observe. Also a new theory needs to be developed as the theory in this paper does not take into account the temporal coherence.

(7.2) Effects of pressure waves and strong winds on barometer data

The following are not alternative models but are points that need careful consideration. First is that the barometer data may contain laterally propagating pressure waves that may lead to an overestimation of pressure sources. Second is the effect of dynamic pressure originated by strong winds.

The reason we are concerned about propagating pressure waves is that if they propagate in the near-surface atmosphere, they should change surface pressure due to its dynamical effects in the atmosphere but they may be a poor source of seismic-wave excitation. Simple transmission of pressure waves into the solid Earth is possible but these pressure waves do not excite seismic waves. If so, our use of barometer data may be an overestimation of pressure as we regard the entire barometer signals as the excitation source. This problem can be solved if we could identify pressure waves and remove them, but identifying pressure waves is not straightforward. This is because because phase information is quite complicated due to a spatially extended source. Therefore, we examined amplitude (PSD) information, such as those in Figure S1. This figure shows amplitude (PSD)-distance plots of pressure for every hour over three days. In going through Figure S1, we noticed some cases that hint towards waves which propagate outward from the center. However, these oscillatory-wave like features occur only in restricted azimuths. In other words, they are not coherent waves that propagate outward from the center. Therefore, these occasional high-amplitude data are not likely to be propagating waves. We believe they are more likely to be stochastic fluctuations in the pressure field. This does not prove that pressure waves in the near-surface atmosphere do not exist but clearly they cannot have much effects on our analysis.

Strong winds may be an important source for the excitation of seismic waves, especially for horizontal-component seismograms as they can apply shear forces directly on the ground. In this paper, we have avoided such a mechanism by analyzing only barometer data and vertical-component seismograms. Even so, strong winds may cause surface pressure changes through its dynamical effects. In order to explain our observation, however, winds should be strong at distant locations from the center and also remain inefficient to excite seismic waves. This may occur but such a scenario appears quite ad hoc. In our next step, we intend to clarify this situation by testing such a mechanism by using wind data and horizontal–component seismograms.

8. Conclusion

Taking advantage of seismic and barometer data from the Earthscope network, we studied the data for Hurricane Isaac (2012) after its landfall. The key observation is that seismic amplitudes (PSD) decay much more quickly than pressure amplitudes (PSD) with distance from the center of this hurricane. In order to explain this observation, we developed a stochastic excitation theory for seismic-wave generation by surface atmospheric pressure changes. We have both the excitation-source information (barometers) and the resultant seismic wave fields (seismometers) from the Earthscope data.

We proposed a model that used the variations in the pressure correlation length to explain the key observational feature. The inverted solutions for the correlation length showed large correlation length close to the center (~ 1-1.5 km at a distance of 70-80 km) and small near-zero correlation length outside of 250 km from the center. The differences in decaying rate are explained by this model.

In our solutions, there is an interesting relation between the pressure and the derived correlation length. Our scaling analysis led to a model in which the excitation source power is proportional to the third power of pressure. This model means that the excitation source becomes stronger near the center of a hurricane; the excitation power becomes more localized closer to the center. Such a centralized source can explain the key observation on the decaying-rate differences.

There may be other mechanisms, however, that can lead to an effectively centralized source. They include higher temporal coherence or frequent transient pressure changes near the center due to strong turbulence. Although we do not see strong evidence for such effects, the current data sets are quite limited due to sparsity near the center; these mechanisms need to be studied more carefully in the future.

Acknowledgments

We thank the three reviewers for comments and suggestions. We particularly thank Victor Tsai for his insightful comments. All Earthscope data were obtained from the data center at IRIS (Incorporated Research Institutions for Seismology). We appreciate their efficient service. This work was supported by a grant from UC Mexus (SB160023).

References

Berg, R. (2013), Tropical Cyclone Report: Hurricane Isaac (AL092012) 21 August – 1 September 2013, NOAA/National Weather Service, Miami, FL.

Bowen, S., J. Richard, J. Mancini, V. Fessatidis, and B. Crooker (2003), Microseism and infrasound generation by cyclones, J. Acoust. Soc. Am., 113, 2562-2573, doi:10.1121/1.1567277.

Bromirski, P. and J. Kossin (2008), Increasing hurricane wave power along the U.S. Atlantic and Gulf coasts, J. Geophys. Res., 113, C07012, doi:10.1029/2007JC004706.

Chi W.-C., W.-J. Chen, B.-Y. Kuo and D. Dolenc (2010), Seismic monitoring of western Pacific typhoons, Mar. Geophys. Res., 31, 239-251, doi:10.1007/s11001-010-9105.x.

Dahlen, A. F. and J. Tromp (1998), *Theoretical Global Seismology*, Princeton University Press, Princeton, New Jersey.

Dziewonski AM, Anderson, Don L. (1981), Preliminary reference Earth model, Phys. Earth Planet. Inter., 25:297--356.

Ebeling C. and S. Stein (2011), Seismological identification and characterization of a large hurricane, B. Seism. Soc. Am., 101, 399-403, doi:10.1785/0120100175.

Edmunds, A. R. (1957), *Angular Momentum in Quantum Mechanics*, Princeton University Press, Princeton, New Jersey.

Emanuel, K.A. (1986), An air-sea interaction theory for tropical cyclones. Part I: Steady state maintenance. *J. Atmos. Sci*., **43**, 585-604.

Emanuel, K.A. (1991), The theory of hurricanes, *Annual Rev. Fluid Mech.,* **23**, 179-196.

Emanuel, K.A. (1997), Some aspects of hurricane inner-core dynamics and energetics. *J. Atmos. Sci*., 54, 1014-1026.

Emanuel, K. (2003), Tropical Cyclones. *Ann Rev. Earth Planet. Sci*., **31**, 75-104

Fukao Y, Nishida K, Suda N, Nawa K, Kobayashi N. (2002), A theory of the Earth's background free oscillations, *J. Geophys. Res.,* 107, B9, 2206, doi:10.1029.

Gilbert, F. (1970), Excitation of the normal modes of the Earth by earthquake sources, *Geophys. J. R. Astr. Soc*., 22, 223-226.

Goldreich, P. and D. A. Keeley (1977), Solar seismology. II. The stochastic excitation of the solar p-modes by turbulent convection, *Astrophys. J*., 212, 243-251.

Gualtieri, L., E. Stutzmann, Y. Capdeville, F. Ardhuin, M. Schimmel, A. Mangeney, and A. Morelli (2013), Modelling secondary microseismic noise by normal mode summation, *Geophys. J. Int*., 193, 1732-1745, doi:10.1093/gji/ggt090.

Hasselmann, K. A. (1963), A statistical analysis of the generation of microseisms, *Rev. Geophys.*, 1, 177-209.

Herron, T. J., I. Tolstoy, and D. W. Kraft (1969), Atmospheric pressure background fluctuations in the mesoscale range, *J. Geophys. Res.,* 74, 1321-1329.

Jorgensen, D. P. (1984), Mesoscale and convective-scale characteristics of mature hurricanes. Part I: General observations by research aircraft, *J. Atmos. Sci.,* 41, 1268-1285.

Jorgensen, D. P., E. Zipser, and M. A. LeMone (1985), Vertical motions in intense hurricanes, *J. Atmos. Sci.,* 42, 839-956.

Kobayashi, N. and K. Nishida (1998), Continuous excitation of planetary free oscillations by atmospheric disturbances, Nature, 395, 357-360.

Lee, W.-D., B.-G. Jo, F. Schwab and S.-B. Jung (2012), Typhoon-generated microseisms observed from the short-period KSRS array, Geosciences Journal, 16, 447-454, doi:10.1007/s12303-01209939-y.

Longuet-Higgins, M. S. (1950), A theory of the origin of microseisms, *Philos. Trans. R. Soc. London, Ser. A*, 243, 1-35.

McDonald, J. A., E. J. Douze, and E. Herrin (1971), The structure of atmospheric turbulence and its application to the design of pipe arrays, *Geophys. J. R. Astr. Soc.*, 26, 99-106.

Nishida, K., Y. Fukao, S. Watada, N. Kobayashi, M. Tahira, N. Suda, K. Nawa, T. Oi and T. Kitajima (2005), Array observation of background atmospheric waves in the seismic band from 1 mHz to 0.5 Hz, Geophys. J. Int., 162, 824-840, doi:10.1111/j.1365-246X.2005.02677.x

Oroville, H. and B. Gutenberg (1946), The use of microseisms in hurricane detection, Transactions, A.G.U., 27, 111-117.

Riehl, H. (1950), A model for hurricane formation, *J. Appl. Phys.,* 21, 917-925.

Tanimoto T. (1999), Excitation of normal modes by atmospheric turbulence, *Geophys. J. Int.,* 136:395--402.

Tanimoto, T. (2005), The Oceanic Excitation Hypothesis for the Continuous Oscillations of the Earth, *Geophys. J. Int.,* 160, 276-288.

Tanimoto, T. (2013), Excitation of microseisms: views from the normal-mode approach, *Geophys. J. Int*., 194, 1755-1759, doi:10.1093/gji/ggt185.

Tanimoto, T. & Um, J. (1999), Cause of continuous oscillations of the Earth, *J. Geophys. Res.,* **104,** 28 723–28 3739.

Tanimoto, T. and A. Lamontagne (2014), Temporal and spatial evolution of an on-land hurricane observed by seismic data, *Geophysical Research Letters*, 41, 7532-7538, doi:10.1002/2014GL061934.

Watada, S., T. Kunugi, K. Hirata, H. Sugioka, K. Nishida, S. Sekiguchi, J. Oikawa, Y. Tsuji and H. Kanamori (2006), Atmospheric pressure change associated with the 2003 Tokachi-Oki earthquake, *Geophys. Res. Lett*., 33, L24306, doi:10.1029/2006GL027967.

Webb, S. C. (2007), The earth’s hum is driven by ocean waves over the continental shelves, *Nature*, 445, 754-756.

Webb, S. C. (2008), The Earth’s hum: the excitation of Earth normal modes by ocean waves, *Geophys. J. Int*., 174, 542-566.

Zhang, J., P. Gerstoft, and P. Bromirski (2010), Pelagic and coastal sources of P-wave microseisms: Generation under tropical cyclones, *Geophys. Res. Lett*., 37, L15301, doi:10.1029/2010GL044288.

Figure Captions:

Figure 1: Track of Hurricane Isaac (August, 2012) and seismic stations from Earthscope (grey triangles). Blue circles indicate when Isaac was a tropical storm, red circles indicate its hurricane stage and green circles are the day markers (00:00 UTC for each day).

Figure 2: (Left-top) Seismic PSD on a map for the frequency range 0.01-0.02 Hz and the location of Hurricane Isaac (red triangle) at UTC 0000, Aug. 30. (Left-bottom) Same seismic data plotted against distance from the hurricane center. A black horizontal dash line indicates the noise level for far-away stations. Same color scale is used for amplitudes. (Right-top) Surface-pressure PSDs from barometer data on a map for 0.01-0.02 Hz for the same time interval with seismic data. (Right-bottom) Pressure PSD plotted against distance from the hurricane center. Three colors are used to denote PSD amplitudes for the top and bottom panels. A dash line shows the noise level.

Figure 3: Seismic PSD vs. distance from the hurricane centers for each time interval. (a) is at UTC 0600, Aug. 29. Data at every six hours are shown in (a)-(g) until UTC 0000, Aug. 31. Vertical long dash lines are at 75 km from the hurricane center.

Figure 4: Pressure PSD vs. distance plots from barometer data. Same time intervals with Figure 3 are shown.

Figure 5: Plot of seismic PSD vs. pressure PSD from the same stations. Stations within 500 km from the hurricane center are plotted for three time intervals, 6:00, 12:00 and 18:00 on August 29. For reference, two line for the power of 1.5 (dash) and 2.0 (blue) are shown. Seismic PSD and pressure PSD are not linear.

Figure 6: Raw and averaged data for UTC 0000, Aug. 30. Seismic data are at top and pressure data are at bottom. Black circles are raw data, blue are averaged data and the red region indicates the interpolated PSDs that we used for analysis.

Figure 7: Summary of the averaged PSDs for seismic data (top) and pressure data (bottom). Results at eight time intervals are shown from UTC 0600, Aug. 29 to UTC 0000, Aug. 31 at every six hours.

Figure 8: Coherence for all pairs of barometric stations within the distance of 1000 km from the hurricane center. Two-hour time intervals were used to compute those results. The correlation length in the atmospheric pressure field is much smaller than the distance scale shown here.

Figure 9a: An example of pressure PSD under the assumption of axisymmetry. For Hurricane Issac, the peak is at about 70-80 km from the center.

Figure 9b: Some examples of kernels $K(x, x_s, \omega)$. Seven curves for x_s = 50-350 km at every 50 km are shown. These kernels are averaged between 0.01 and 0.02 Hz.

Figure 10a-10d: (a) Results of inversion for the correlation length. Correlation length is in the top panel with error bars, seismic PSD are in the second panel, and pressure PSD is in the bottom panel. Fitting is done for seismic PSD where the data are red and theoretical fit is in dashed blue (middle panel). This is at 0600, Aug. 29. (b) Same with (a) except that these are at UTC 1200, Aug. 29. (c) Same with (a) except that they are at UTC 1800, Aug. 29. (d) Same with (a) except that they are at UTC 0000, Aug. 30.

Figure 11: Examples of the trade-off curves for the inversions in Figure 8. The top panel is for UTC 0600 Aug. 29 and the bottom is for UTC 1200, Aug. 29. The solution norms are plotted against the misfit in seismic PSD data. The red circles are the selected values.

Figure 12: Plot of the correlation lengths vs. the pressure PSD for three different cases of damping parameters. From top to bottom, the damping parameter was varied by a factor of 100 (0.01-0.1-1.0). Lines are the least squares fit to data. The main point of this figure is the relatively stable coefficient of about 0.5 in the least squares formula. In this formula, y is the logarithm of pressure and x is the logarithm of L^2.

Figure 13: (a) Comparison between theory and data for the cubic model. There are some scatters but the cubic model seems to explain the overall trend in data. (b) The cubic model was re-derived by fitting the data (same data with the bottom panel in Figure 12) by fixing the gradient as 0.5. This means that there is a relation between the correlation length and pressure PSD as $L = (1/714.8)S_p$ (see text).

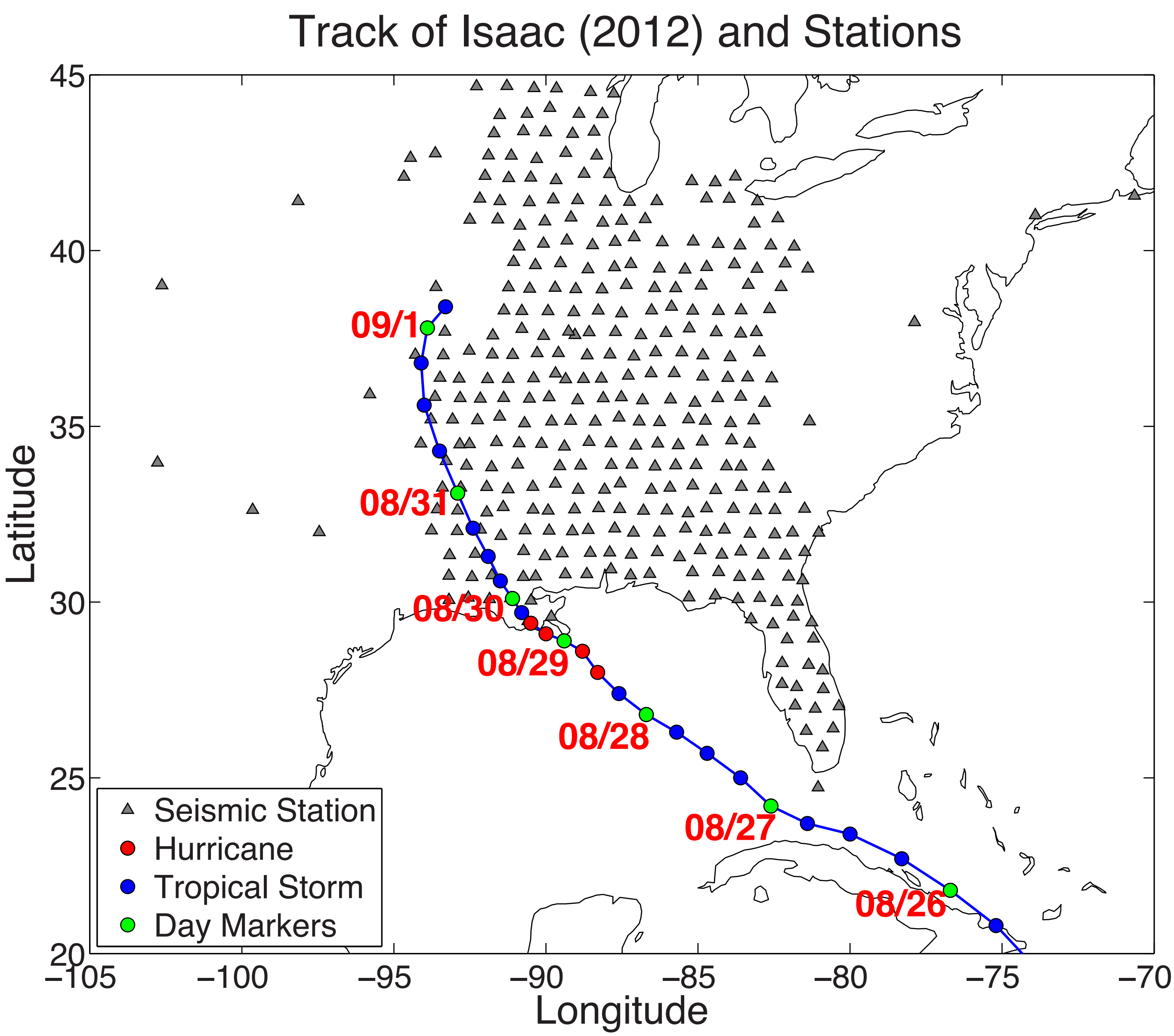
Track of Isaac (2012) and Stations
45
40
35
30
25
20
−105
−100
−95
−90
−85
−80
−75
−70
Latitude
Longitude
09/1
08/31
08/30
08/29
08/28
08/27
08/26
Seismic Station
Hurricane
Tropical Storm
Day Markers

Figure 1

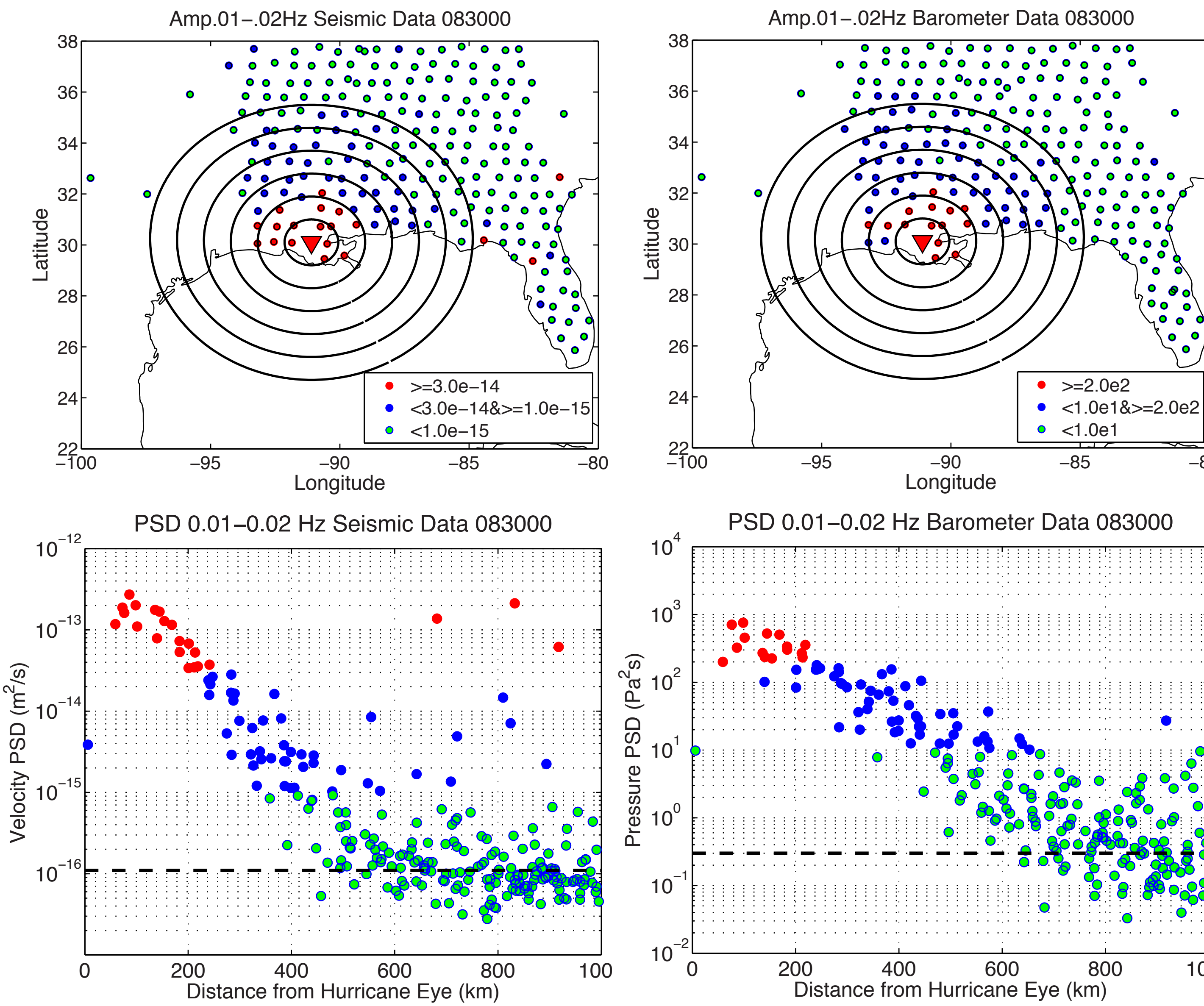

Amp.01−.02Hz Seismic Data 083000
Latitude
Longitude
>=3.0e−14
<3.0e−14&>=1.0e−15
<1.0e−15
Amp.01−.02Hz Barometer Data 083000
>=2.0e2
<1.0e1&>=2.0e2
<1.0e1
PSD 0.01−0.02 Hz Seismic Data 083000
Velocity PSD (m²/s)
Distance from Hurricane Eye (km)
PSD 0.01−0.02 Hz Barometer Data 083000
Pressure PSD (Pa²s)

Figure 2

Seismic Data

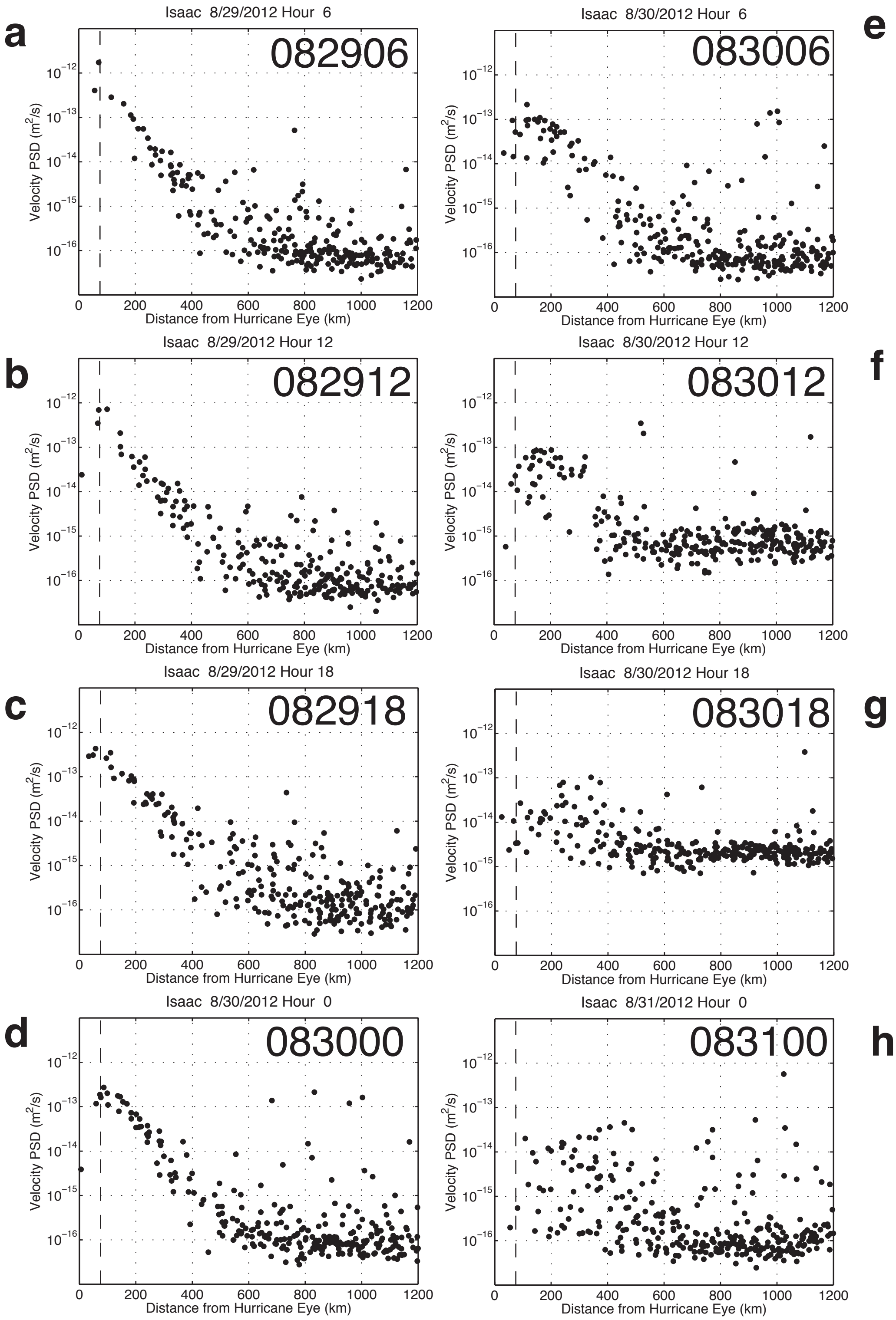

Figure 3

Barometer Data

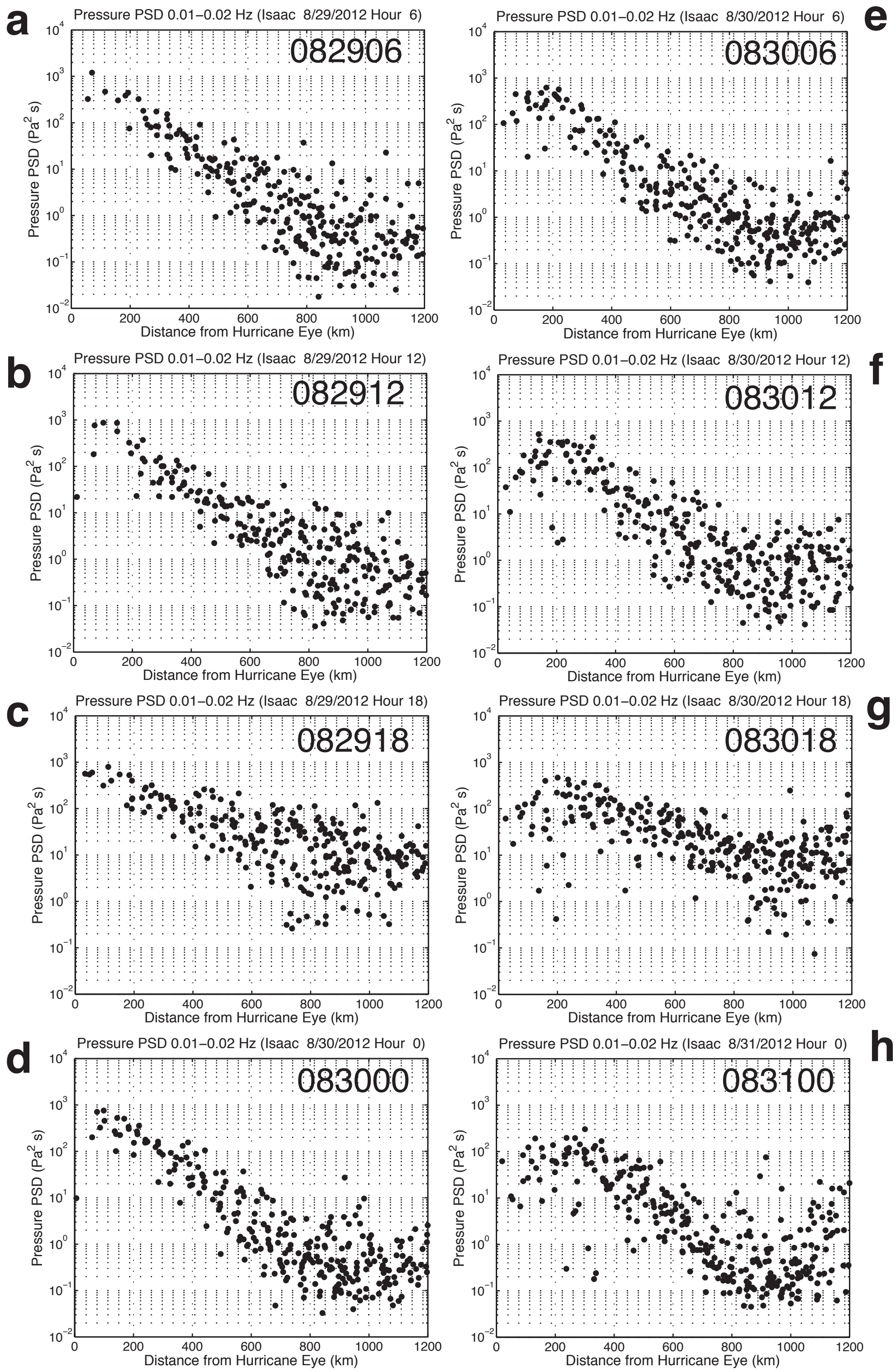

Figure 4

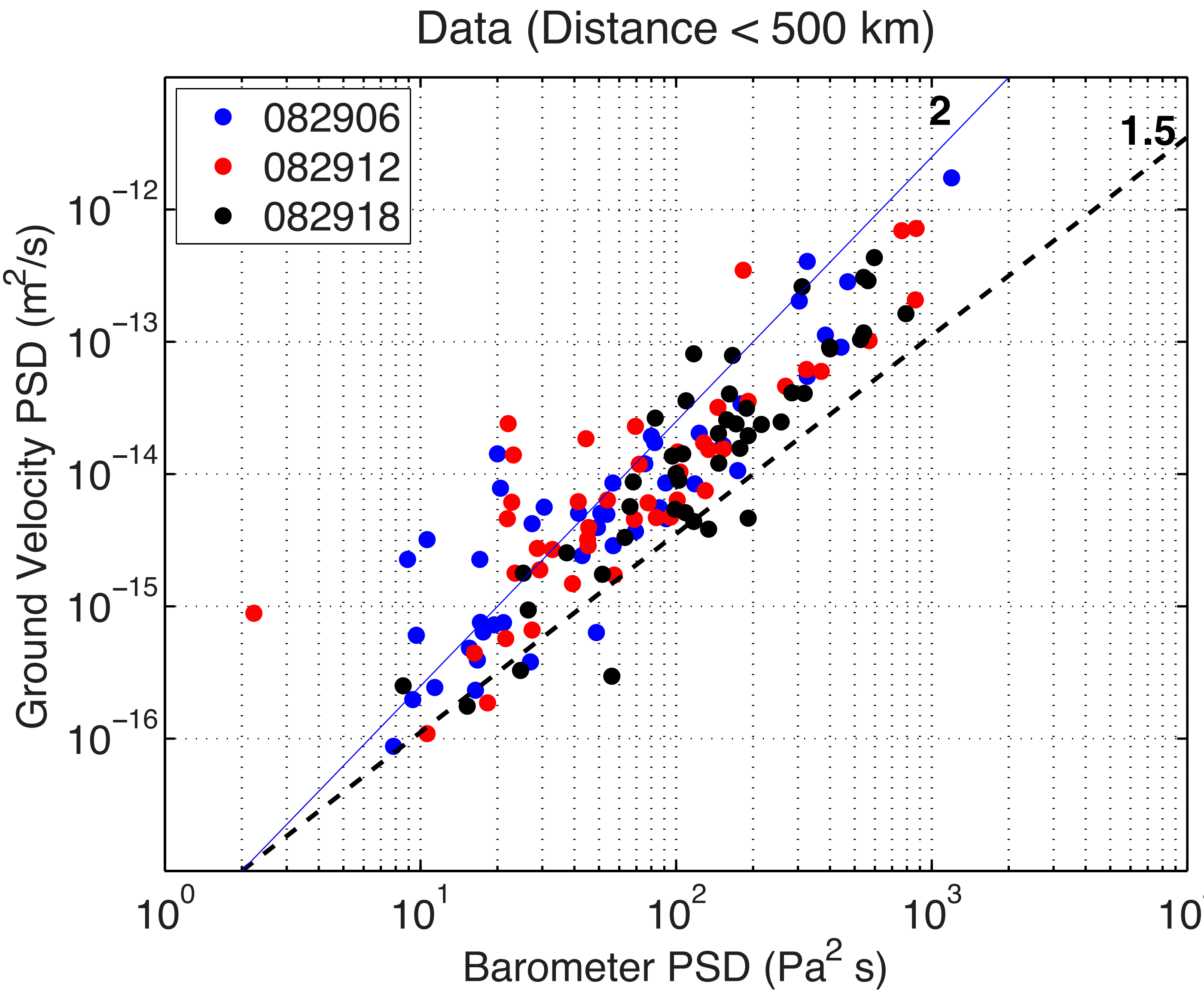

Data (Distance < 500 km)
082906
082912
082918
2
1.5
10^{-12}
10^{-13}
10^{-14}
10^{-15}
10^{-16}
Ground Velocity PSD (m^2/s)
10^0
10^1
10^2
10^3
10^4
Barometer PSD (Pa^2 s)

Figure 5

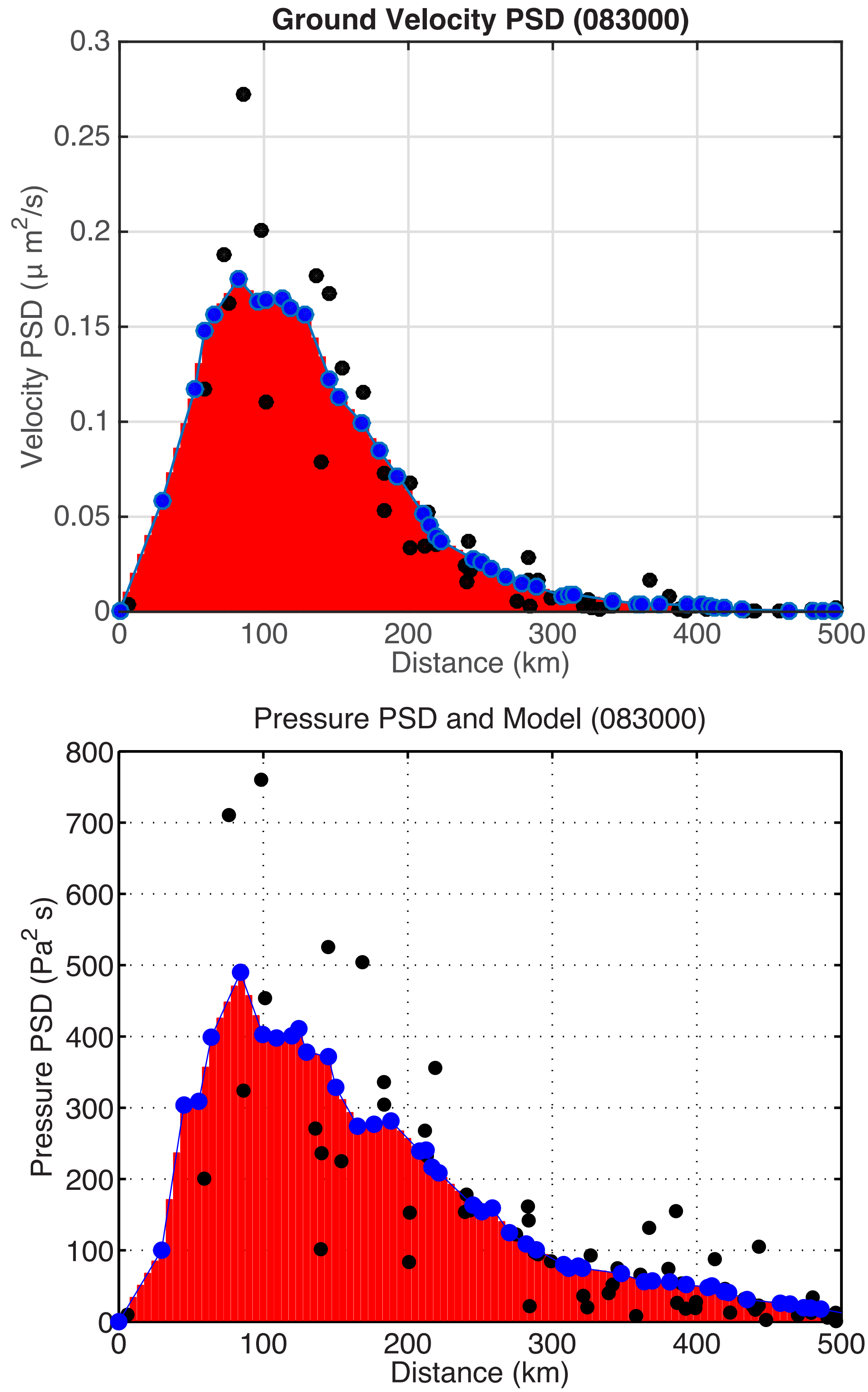
Ground Velocity PSD (083000)
Velocity PSD (μ m^2/s)
Distance (km)
Pressure PSD and Model (083000)
Pressure PSD (Pa^2 s)
Distance (km)

Figure 6

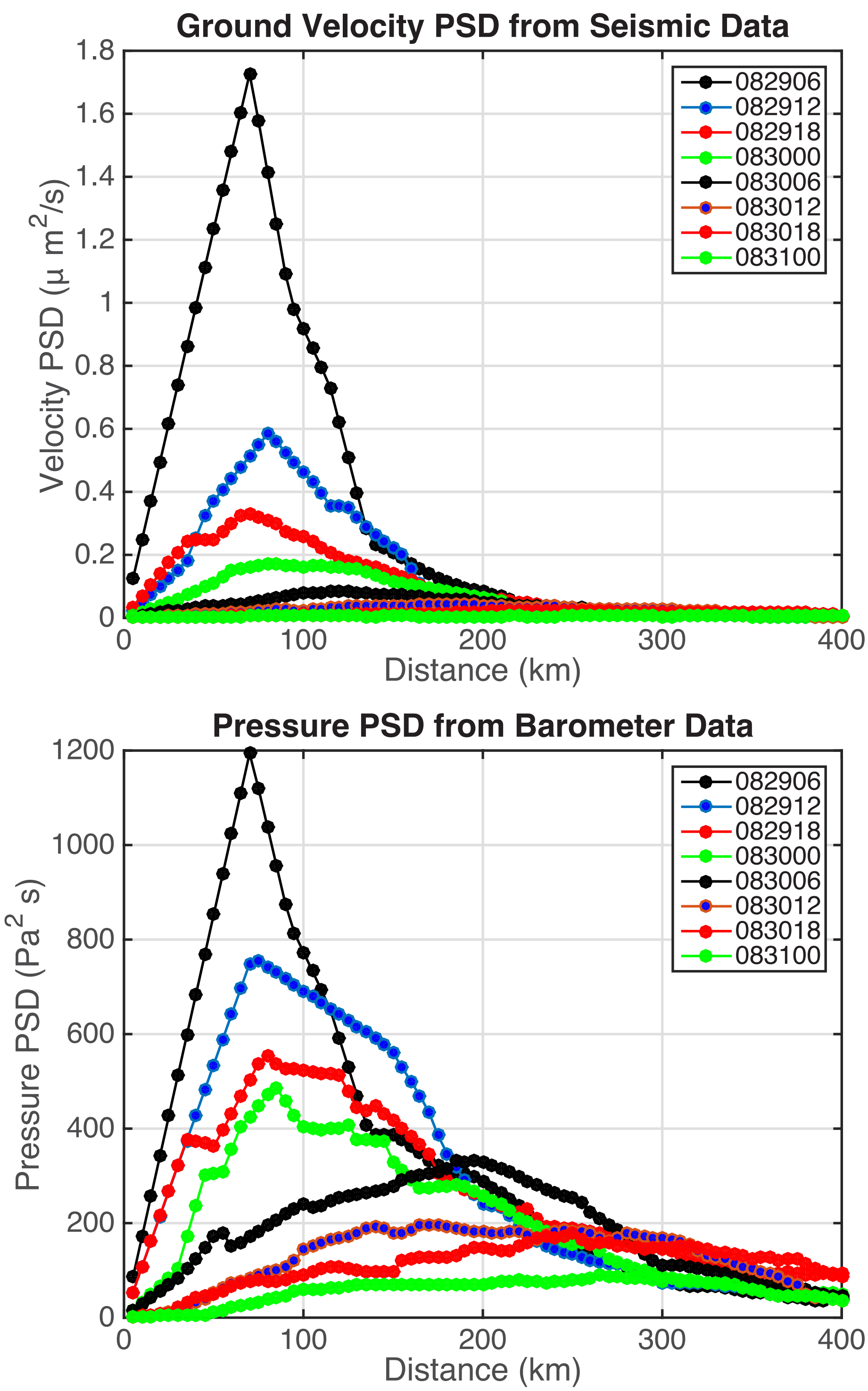
Ground Velocity PSD from Seismic Data
Velocity PSD (μ m²/s)
Distance (km)
082906
082912
082918
083000
083006
083012
083018
083100
Pressure PSD from Barometer Data
Pressure PSD (Pa² s)
Distance (km)
082906
082912
082918
083000
083006
083012
083018
083100

Figure 7

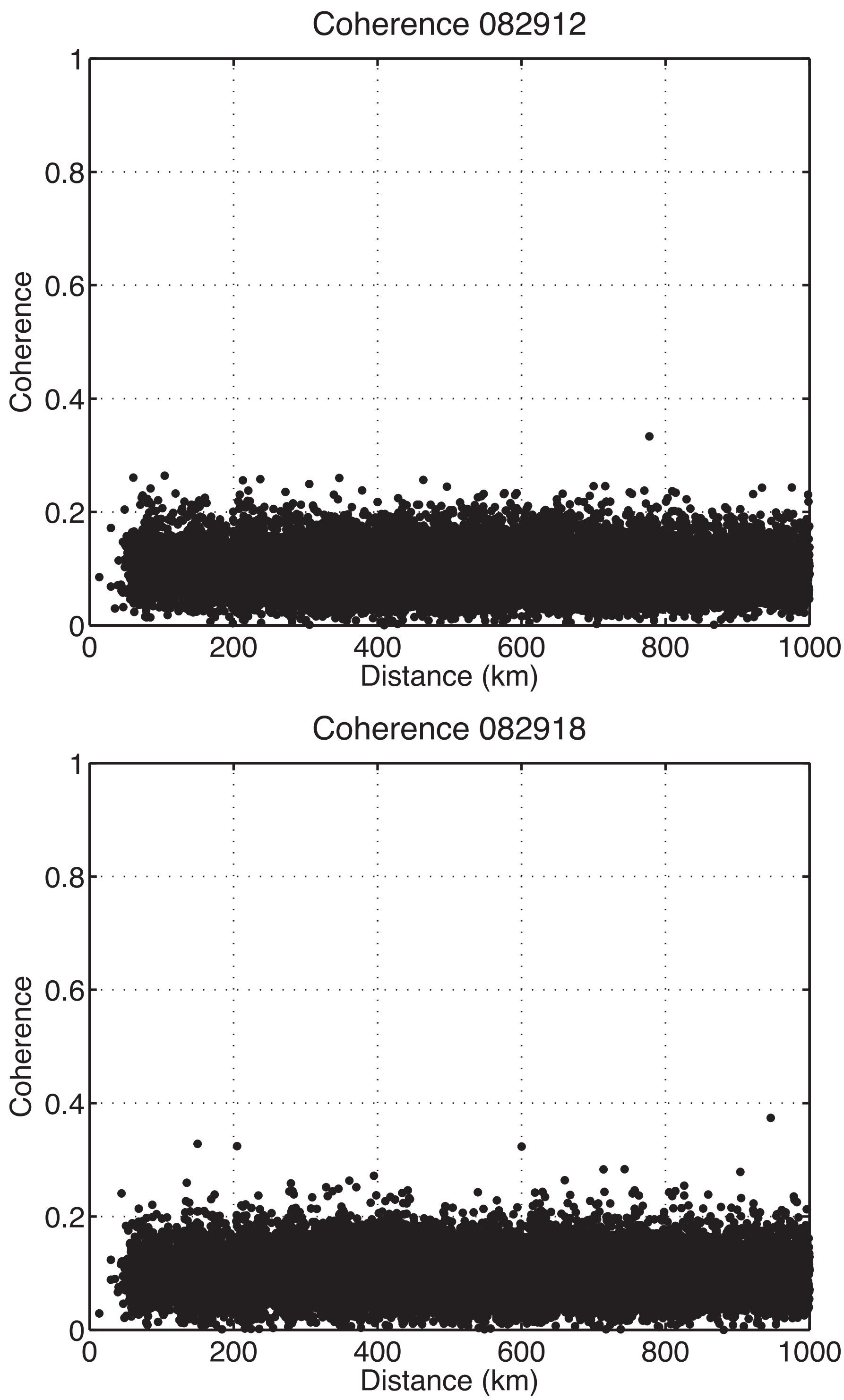
Coherence 082912
Coherence
Distance (km)
Coherence 082918
Coherence
Distance (km)
0
0.2
0.4
0.6
0.8
1
0
200
400
600
800
1000

Figure 8

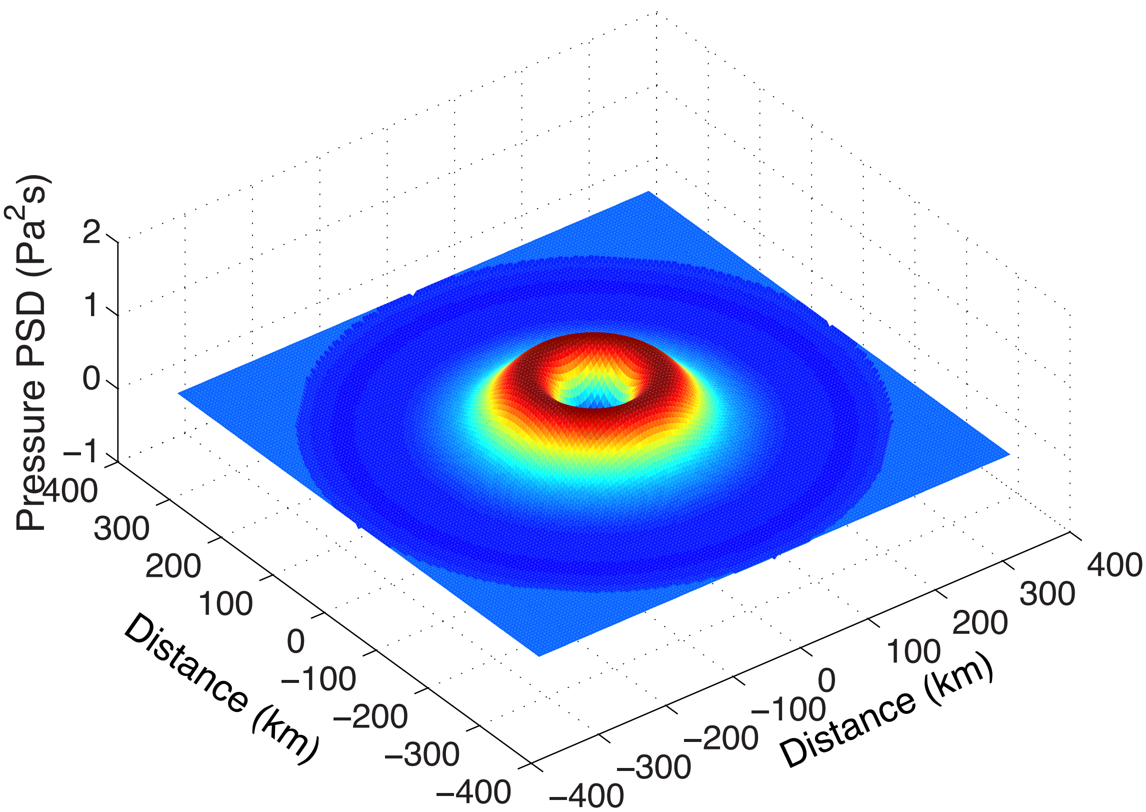

Pressure PSD (Pa^2s)
2
1
0
−1
400
300
200
100
0
−100
−200
−300
−400
Distance (km)
−400
−300
−200
−100
0
100
200
300
400
Distance (km)

Figure 9a

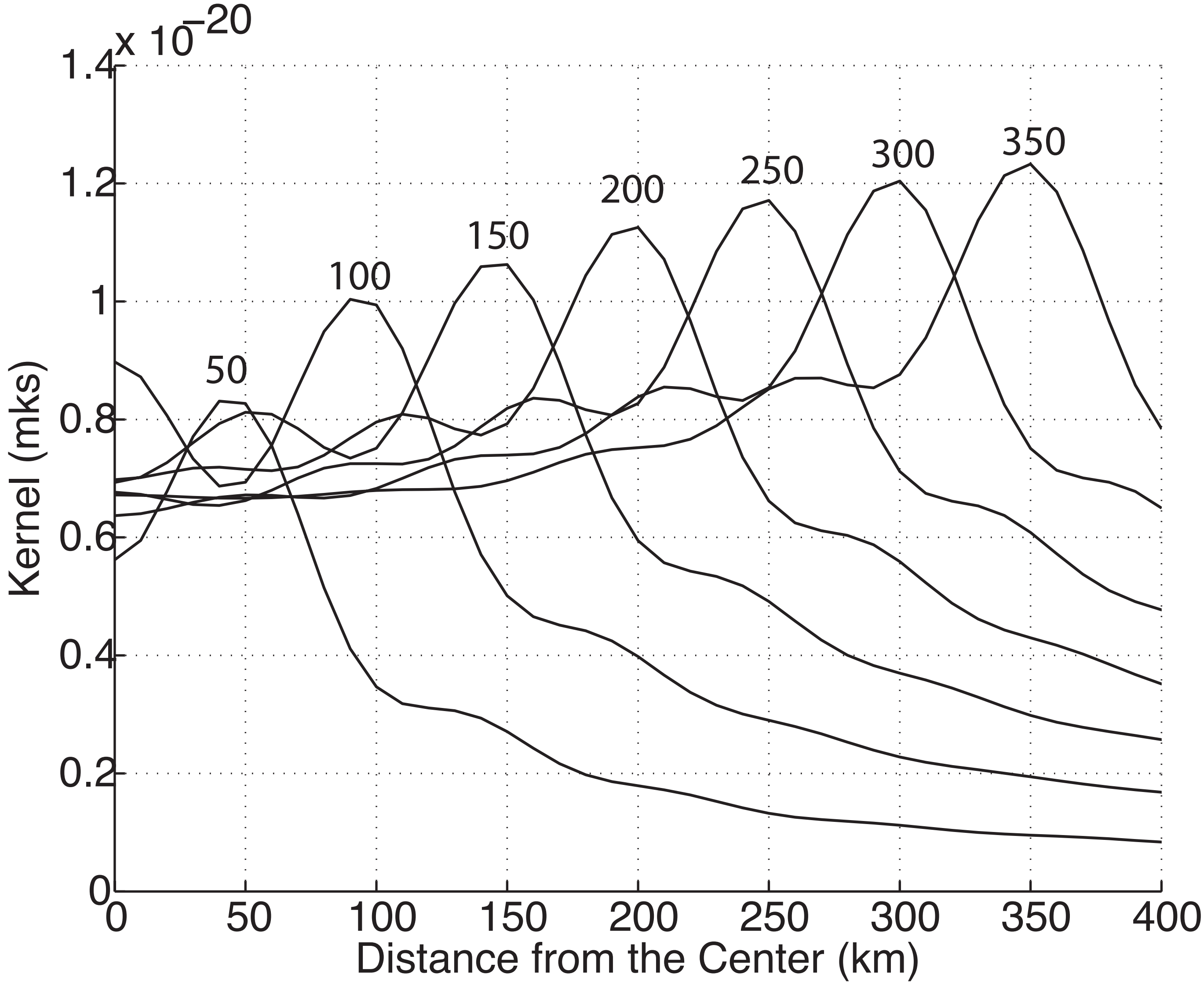
x 10^-20
1.4
1.2
1
0.8
0.6
0.4
0.2
0
Kernel (mks)
50
100
150
200
250
300
350
0
50
100
150
200
250
300
350
400
Distance from the Center (km)

Figure 9b

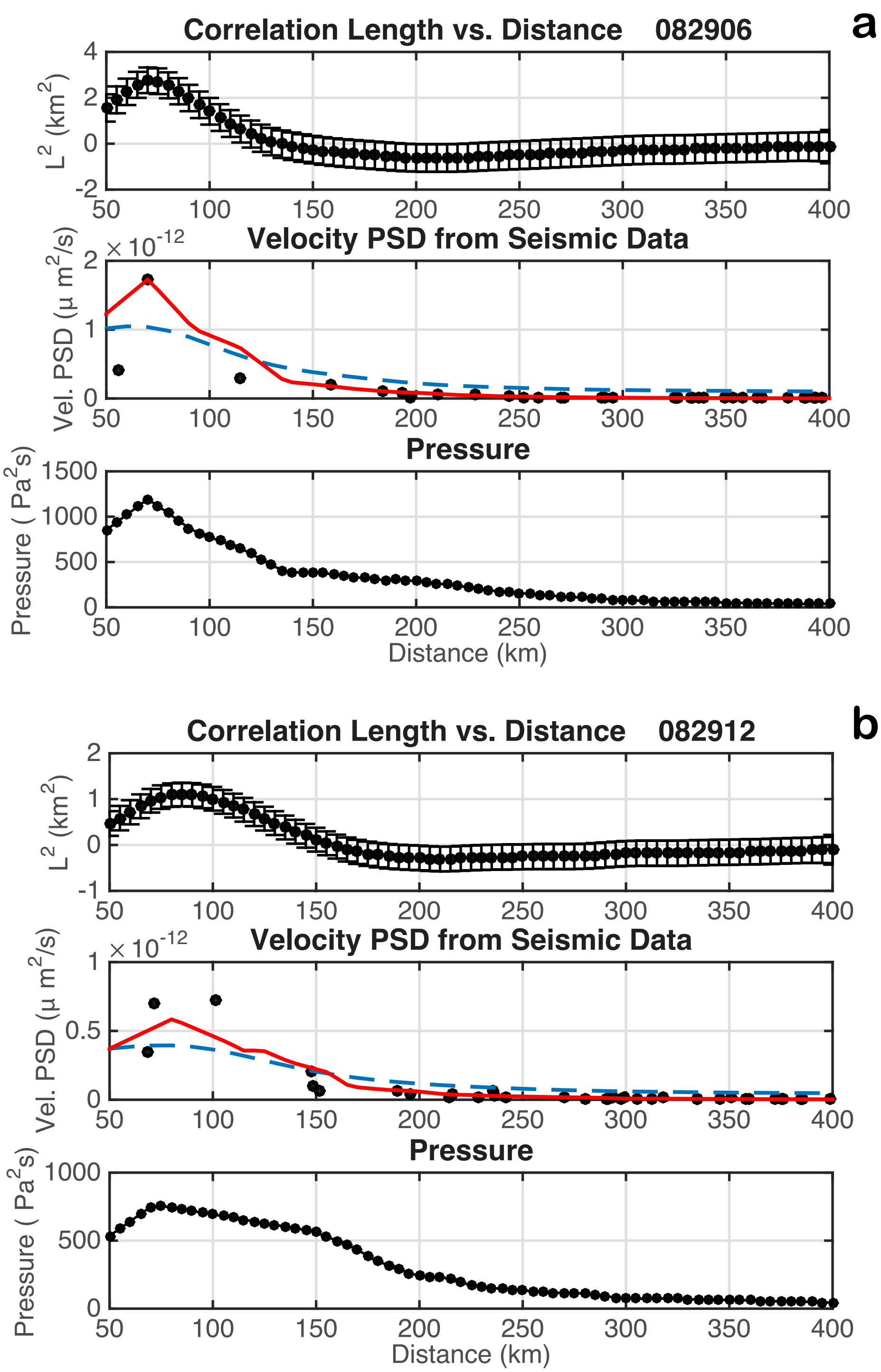
a
Correlation Length vs. Distance 082906
L^2 (km^2)
Velocity PSD from Seismic Data
×10^-12
Vel. PSD (μ m^2/s)
Pressure
Pressure (Pa^2s)
Distance (km)
b
Correlation Length vs. Distance 082912
L^2 (km^2)
Velocity PSD from Seismic Data
×10^-12
Vel. PSD (μ m^2/s)
Pressure
Pressure (Pa^2s)
Distance (km)

Figure 10 (a+b)

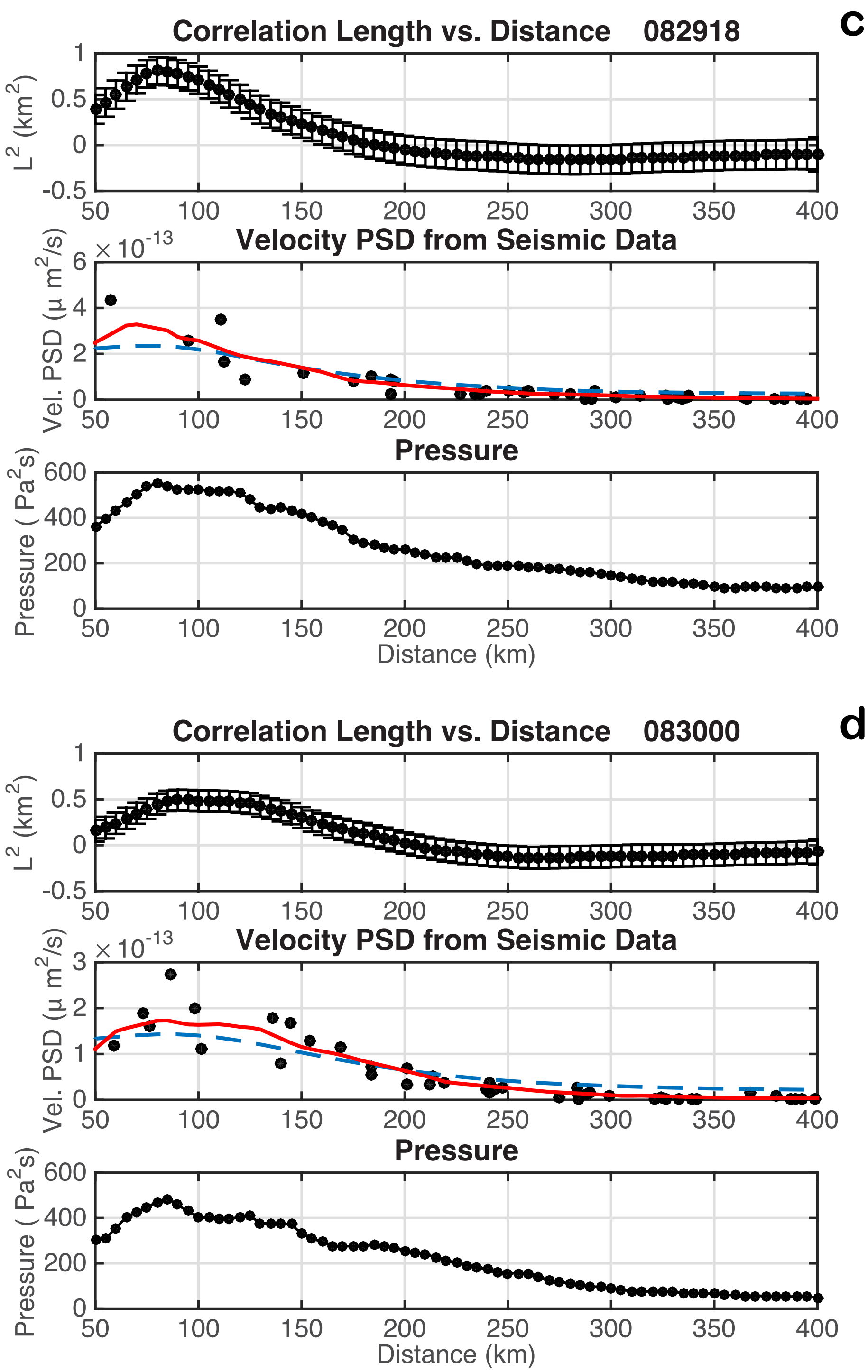
c
Correlation Length vs. Distance 082918
L^2 (km^2)
Velocity PSD from Seismic Data
×10^-13
Vel. PSD (μ m^2/s)
Pressure
Pressure (Pa^2s)
Distance (km)
d
Correlation Length vs. Distance 083000
L^2 (km^2)
Velocity PSD from Seismic Data
×10^-13
Vel. PSD (μ m^2/s)
Pressure
Pressure (Pa^2s)
Distance (km)

Figure 10 (c+d)

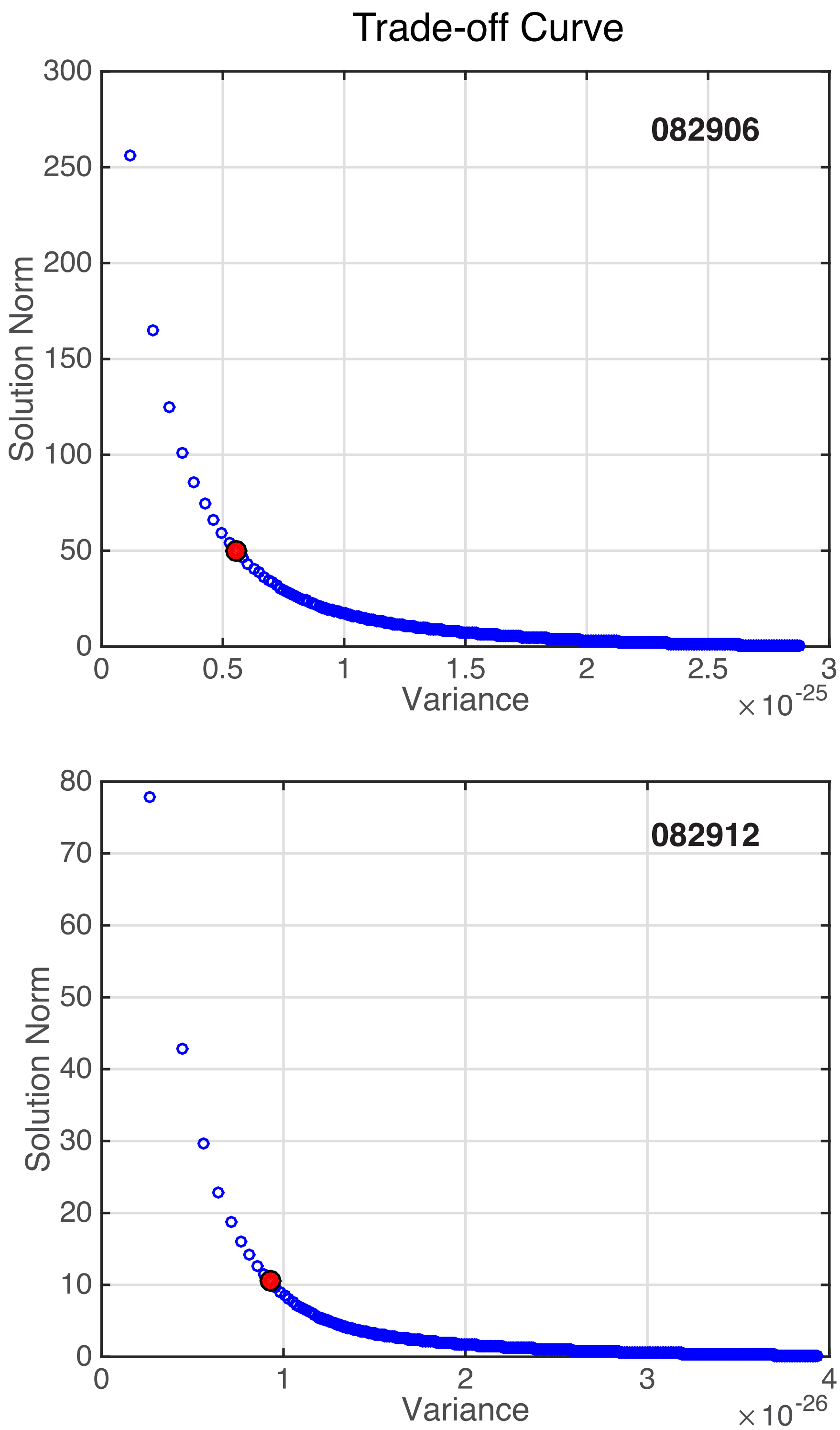

Trade-off Curve
082906
Solution Norm
Variance
$\times 10^{-25}$
082912
Solution Norm
Variance
$\times 10^{-26}$

Figure 11

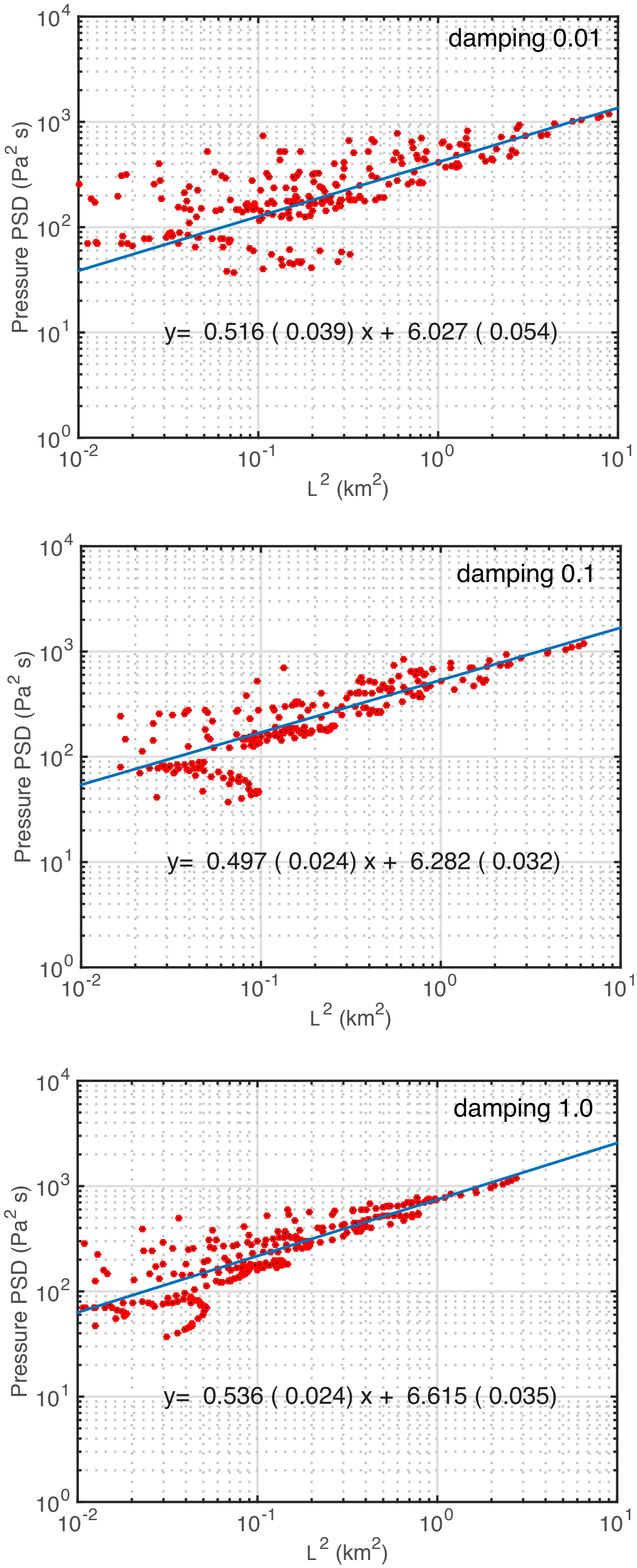
damping 0.01
y= 0.516 (0.039) x + 6.027 (0.054)
Pressure PSD (Pa^2 s)
L^2 (km^2)
damping 0.1
y= 0.497 (0.024) x + 6.282 (0.032)
Pressure PSD (Pa^2 s)
L^2 (km^2)
damping 1.0
y= 0.536 (0.024) x + 6.615 (0.035)
Pressure PSD (Pa^2 s)
L^2 (km^2)

Figure 12

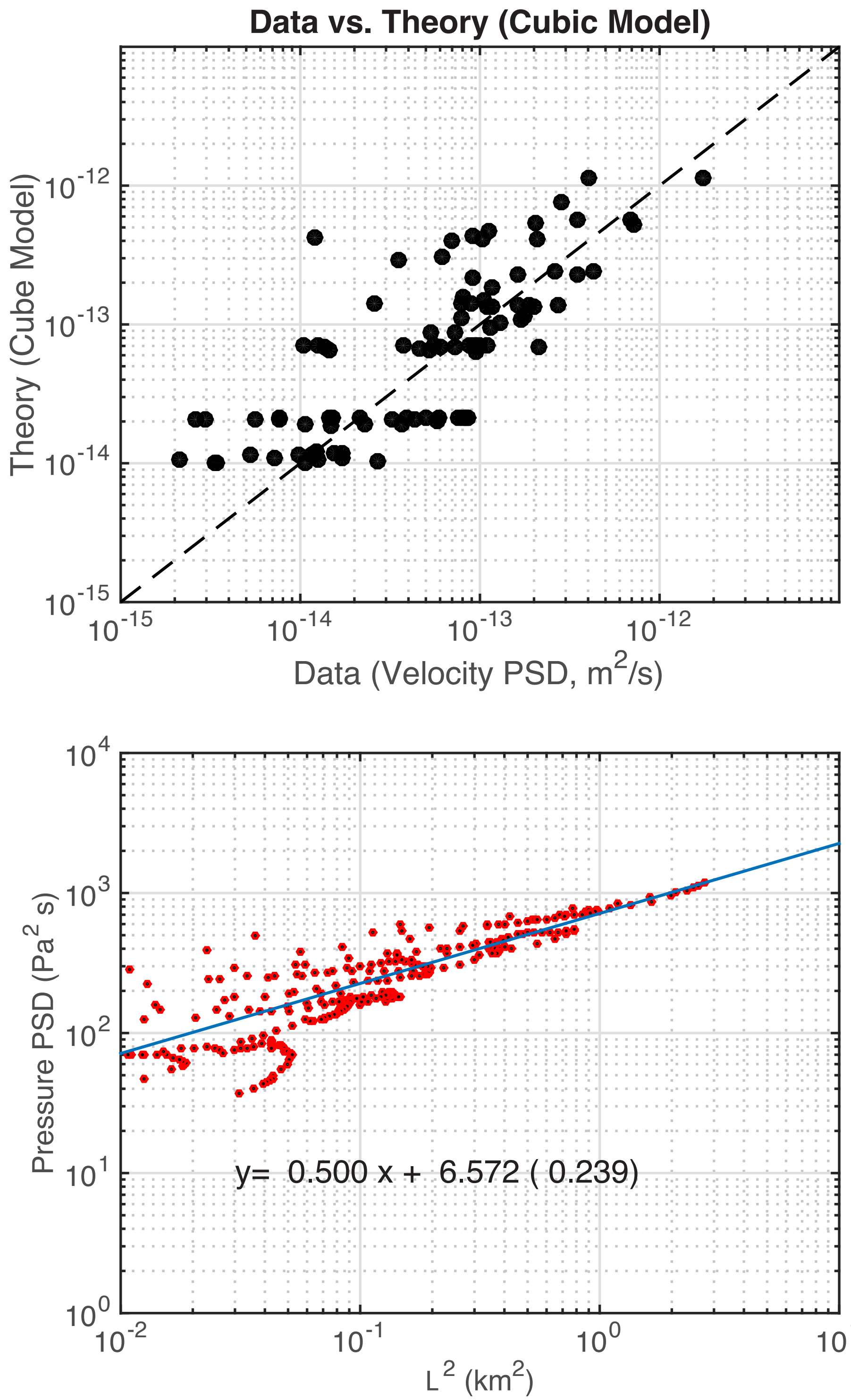
Data vs. Theory (Cubic Model)
Theory (Cube Model)
Data (Velocity PSD, m2/s)
Pressure PSD (Pa2 s)
y= 0.500 x + 6.572 (0.239)
L2 (km2)

Figure 13